

# The Variable Stars and Blue Horizontal Branch of the Metal-Rich Globular Cluster NGC 6441

Andrew C. Layden<sup>1,2,3</sup>, Laura A. Ritter

Department of Astronomy, University of Michigan, Ann Arbor, MI 48109-1090, U.S.A.

Douglas L. Welch<sup>1</sup>, Tracy M. A. Webb<sup>1</sup>

Department of Physics & Astronomy, McMaster University, Hamilton, Ontario L8S 4M1, Canada

## ABSTRACT

We present time-series  $VI$  photometry of the metal-rich ( $[Fe/H] = -0.53$ ) globular cluster NGC 6441. Our color-magnitude diagram shows that the extended blue horizontal branch seen in *Hubble Space Telescope* data exists in the outermost reaches of the cluster. About 17% of the horizontal branch stars lie blueward and brightward of the red clump. The red clump itself slopes nearly parallel to the reddening vector. A component of this slope is due to differential reddening, but part is intrinsic. The blue horizontal branch stars are more centrally concentrated than the red clump stars. We have discovered  $\sim 50$  new variable stars near NGC 6441, among them eight or more RR Lyrae stars which are very probably cluster members. Comprehensive period searches over the range 0.2–1.0 days yielded unusually long periods (0.5–0.9 days) for the fundamental pulsators compared with field RR Lyrae of the same metallicity. Three similar long-period RR Lyrae are known in other metal-rich globulars. With over ten examples in hand, it seems that a distinct sub-class of RR Lyrae is emerging. It appears that these stars have the same intrinsic colors as normal RR Lyrae. Using the minimum-light color of the RR Lyrae, we determine the mean cluster reddening to be  $E(B - V) = 0.45 \pm 0.03$  mag, with a significant variation in reddening across the face of the cluster. The observed properties of the horizontal branch stars are in reasonable agreement with recent models which invoke deep mixing to enhance the atmospheric helium abundance, while they conflict with models which assume high initial helium abundance. The light curves of the c-type RR Lyrae seem to have unusually long rise times and sharp minima. Reproducing these light curves in stellar pulsation models may provide another means of constraining the physical variables responsible for the anomalous blue horizontal branch extension and sloped red clump observed in NGC 6441.

---

<sup>1</sup>Visiting Astronomer, Cerro Tololo Inter-American Observatory. CTIO is operated by AURA, Inc. under contract to the National Science Foundation.

<sup>2</sup>Hubble Fellow.

<sup>3</sup>Current address: Dept. of Physics & Astronomy, Bowling Green State Univ., Bowling Green, OH 43403, U.S.A.

*Subject headings:* color-magnitude diagrams — globular clusters: individual (NGC 6441) — RR Lyrae variable — stars: horizontal-branch — stars: variables: general

## 1. Introduction

The canonical metal-rich globular cluster ( $[Fe/H] > -0.8$ ) has a horizontal branch (helium core burning phase of stellar evolution) which is compressed against the red giant branch to form a “red clump” (e.g., 47 Tuc, Carney et al. 1993; M 71, Hodder et al. 1992). Standard stellar evolution theory and synthetic horizontal branches confirm this morphology (e.g., Lee et al. 1990, Dorman 1992). However, it is becoming clear that the situation is more complicated than this canonical picture would have us believe.

First, it is evident that a significant fraction of the RR Lyrae variable stars (horizontal branch stars lying in the pulsation instability strip, hereafter RRL) in the field near the Sun are metal-rich. Preston (1959) first recognized this fact, and the recent metallicity distribution of Layden (1994) shows that 22% of the field RR Lyrae within 2 kpc of the Sun have  $[Fe/H] > -1.0$ , and 9% have  $[Fe/H] > -0.5$  dex. Furthermore, the kinematics of these stars identify them with the Galaxy’s thick disk population, and a few RRL with abundances approaching solar may be produced by the thin disk (Layden 1995a). The standard horizontal branch star picture does not explain the presence of stars hot enough to lie in the instability strip at these ages and metallicities.

In addition, several metal-rich globular clusters contain one or more RRL candidates (cf. Suntzeff et al. 1991). Note however that the often-quoted example, V9 in 47 Tucanae, has an anomalously high luminosity and long period compared with field RRL of similar abundance (Carney et al. 1993). Nevertheless, Layden (1995b) showed that the number of RRL per unit progenitor luminosity was roughly equal between the metal rich thick disk field and globular cluster populations. This comparison was hampered by the incomplete search for RRL among the population of metal-rich globulars.

A second important complication to the canonical picture of metal-rich globular cluster horizontal branches (HBs) is the recent observation of blue HBs in two globulars, and in several open clusters. *Hubble Space Telescope* observations by Rich et al. (1997) showed the globulars NGC 6388 and 6441 ( $[Fe/H] = -0.60$  and  $-0.53$ ) to have long blueward extensions to their otherwise red HBs. They initially suggested that age or dynamical effects could be responsible for the blue HBs. However, no deep photometry has been published for these clusters to constrain their ages, and calculations by Rich et al. (1997) indicated that stellar interactions are too infrequent to be the culprit. They left open the question of the physical cause of the phenomenon. Blue HB stars in younger, more metal-rich open clusters have also been observed (e.g., NGC 6791, Liebert et al. 1994).

Theoretical studies are also focusing on the blue HB star problem. Sweigart & Catelan (1998) presented three scenarios involving enhanced helium abundance and/or stellar rotation designed to explain the blue HB observations of Rich et al. (1997). They emphasized that observational tests including the existence and periods of RR Lyrae variables, and the relative numbers of HB and red giant branch stars (the *R*-ratio), could discriminate between their scenarios. They suggest that the blue HB extensions seen by Rich et al. (1997) are extreme cases of the “Second Parameter Effect”, in which the color distribution of stars along globular cluster HBs is seen to depend on metallicity and a second parameter, possibly age, Helium or CNO abundances, or core rotation.

Thus, ample motivation exists to study the horizontal branches and RR Lyrae content of metal-rich globular clusters. With this in mind, we have undertaken a variable star survey of twelve of the metal-rich globulars listed by Suntzeff et al. (1991) as having poor or no variable star searches. In this paper, we report our results for the first cluster, NGC 6441. If dynamical effects are involved, the high luminosity and central concentration of this cluster (Harris 1996) make it among the most likely to harbor RRL. This prospect is enhanced by the presence of the blue HB stars observed by Rich et al. (1997). The best existing ground-based photometry of NGC 6441 is the photographic work of Hesser & Hartwick (1976), which reached only the brightest stars on the horizontal branch.

In §2 of this paper, we describe the observation and data reduction procedures we employed. In §3 we present color-magnitude diagrams of the cluster and nearby field. In §4 we identify  $\sim 50$  variable stars in the cluster, derive their photometric properties, and for some present their mean light curves. In §5 we derive the foreground reddening of NGC 6441 and discuss in detail the properties of the cluster’s RR Lyrae variables and compare them to the predictions of the Sweigart & Catelan (1998) models. We present our conclusions in §6, and in the Appendix we note details on some of the variable stars.

## 2. Observations and Reductions

We obtained time-series images of NGC 6441 using the direct CCD camera on the 0.9-m telescope at Cerro Tololo Inter-American Observatory during two runs in May and June of 1996 (3 and 8 usable nights, respectively). The Tek#3 2048 CCD provided a 13.5 arcmin field of view with 0.4 arcsec pixels. We used filters matched to the CCD to reproduce the Johnson *V* and Kron-Cousins *I* bandpasses. We processed the raw images by following the usual procedure for overscan subtraction and bias correction, and we used twilight sky frames to flat-field the data.

In each pointing toward the cluster, we obtained a short exposure (30–100 sec) *VI* frame pair and a long exposure (250–300 sec) *VI* pair. This provided two independent magnitude estimates of the HB stars at each observational epoch, and extended the dynamical range of the observations. Such pointings were obtained 0–3 times each night. The time interval between pointings was at least 2 hours, so a typical RR Lyrae (0.3–0.8 day periods) would undergo a significant magnitude

change. In total, we obtained 15 pointings toward NGC 6441. The seeing varied between 1.2 and 3.0 arcsec (median 1.7 arcsec). Figure 1 shows a short-exposure  $V$ -band image of the cluster. The bright star to the West of the cluster was masked out in all the frames.

On a photometric night in May 1996, we obtained a  $VI$  image pair of NGC 6441, together with a large number of Landolt (1992) photometric standards. We also secured an off-cluster  $VI$  pair centered 13.3 arcmin North of the cluster center, outside the tidal radius (7.8 arcmin, Harris 1996) designed to determine the photometric properties of the fore/background starfield. The standards covered a large range in color ( $-0.3 < V - I < 4.0$ ) and airmass ( $1.08 < X < 1.74$ ), and were obtained at roughly hourly intervals throughout the night. This time ( $T$ ) coverage confirmed that the entire night was photometric, and enabled us to seek and correct for small, slow variations in extinction. In total, 63 individual standards were observed at 13 independent epochs. The instrumental aperture magnitudes of these stars ( $A_b$ ), in bandpasses  $b = V$  or  $I$ , were fit with the equation

$$A_b - S_b = c_{1,b} + c_{2,b}X + c_{3,b}(V - I) + c_{4,b}T + c_{5,b}T^2$$

where  $S_b$  is the standard magnitude and  $c_{i,b}$  ( $i = 1, 5$ ) are the fitted coefficients. The time-dependent terms produced corrections of 0.01 mag or less. The rms scatter about the adopted fits were 0.010 and 0.013 mag in  $V$  and  $I$ , respectively.

The on- and off-cluster  $VI$  pairs obtained on this night were reduced using the DAOPHOT II point spread function (PSF) fitting photometry package (Stetson 1994). The interactivity of this package enabled us to select  $\sim 170$  PSF stars well-distributed spatially over the frame. This was critical in accurately characterizing the significant radial variation in PSF across the frame. For each frame, the PSF was iteratively improved by fitting and removing faint neighbor stars. The final PSF was applied to the image using ALLSTAR. A second application of ALLSTAR yielded a frame with all the stars subtracted except a set of  $\sim 220$  bright, isolated stars. This frame was used to derive aperture corrections by subtracting the PSF-fit DAOPHOT magnitudes of the stars from their aperture magnitudes (derived using the same software and parameters as those used in measuring the standard stars). The aperture correction was then applied to all the stars measured in the frame, and the standard star relations were applied, yielding standard  $VI$  magnitudes for thousands of stars on the on- and off-cluster fields. The on-cluster  $VI$  data provides a set of secondary standards for calibrating the other on-cluster images.

The remaining images of NGC 6441 were reduced using a version of the DoPHOT PSF-fitting package (Schecter, Mateo, & Saha 1993) which allows for spatial variations in the PSF. Instrumental magnitudes were obtained for each frame and combined into instrumental  $VI$  pairs, and then transformed to standard  $VI$  magnitudes via fits to the secondary standards described above. We grouped the  $VI$  frame pairs as follows: good-seeing frames with (a) long, and (b) short exposure times, and poor-seeing frames with (c) long, and (d) short exposure times. This grouping strategy minimized mis-matches due to variable depth and seeing. Within each group, we spatially matched stars from the different frames, and combined the photometry for each star using an error-weighted mean. For the error in each combined stellar magnitude, we adopted the

standard error of the mean for the individual measures, which proved to be a more conservative estimate than computing the error directly from the DoPHOT errors.

### 3. Color-Magnitude Diagrams

We combined the mean photometry from groups *a* and *b* (the long- and short-exposure frames with good seeing) using an error-weighted mean to produce a single dataset with maximum dynamic range. Outside a radius of 1100 pix (7.33 arcmin) from the cluster center, elongated star images sometimes registered as multiple stars, compromising the mean photometry and complicating variable star detection (see §4). Figure 2a shows the  $(V - I, V)$  color-magnitude diagram (CMD) for 22,871 stars on the on-cluster frame lying within 1100 pix of the cluster center. Only stars detected on four or more frames, and having combined errors in  $V$  and  $V - I$  of  $\sigma_V < 0.050$  mag and  $\sigma_{V-I} < 0.071$  mag, are shown. Table 1 lists the combined photometry for all the bright stars ( $V < 19$  mag) within 1100 pix of the cluster center.

Figure 2b shows the corresponding CMD for the off-cluster field. This diagram represents data from a single  $VI$  frame pair, so the errors are larger. Poor photometry, galaxies, and cosmic rays were rejected by performing 3- $\sigma$  cuts on the DAOPHOT values of “ $\chi$ ” and “sharp” as functions of magnitude. Only stars with  $\sigma_V < 0.050$  mag and  $\sigma_{V-I} < 0.071$  mag are shown (DAOPHOT errors).

Several features are apparent in these CMDs. First, both the cluster and field have large numbers of extremely red giant stars. Second, in both CMDs one can detect the red clump stars of the bulge at  $V \approx 17$  and  $V - I \approx 1.7$  mag. This agrees well with photometry of the nearby field MM-5B from the OGLE group (Stanek et al. 1994). Note that the red clump in Figure 2b is shifted redward and faintward relative to that in Figure 2a, suggesting a mean reddening difference between the two fields. Third, a prominent feature of the on-cluster CMD is the NGC 6441 red clump, which forms a swath of stars near  $V \approx 17.5$  and  $V - I \approx 1.5$  mag, running parallel to the reddening vector (we adopt  $A_V = 2.6 E(V - I)$  throughout this paper). Finally, the on-cluster CMD shows a population of stars bluer and somewhat brighter than the cluster red clump. Such stars are not present on the off-cluster CMD, and represent the first ground-based view of the extended blue horizontal branch seen by Rich et al. (1997).

Figures 3a and 3b zoom in on the HB regions of these CMDs. The tight distribution of red clump stars in Figure 3a paralleling the reddening vector suggests that there is significant differential reddening across the face of the cluster. This also explains why a tight red giant branch (RGB) is not seen; differential reddening spreads the RGB stars roughly perpendicular to the un-reddened RGB fiducial. We will consider the reddening problem in more detail in §5.2.

Another important feature is highlighted in Figure 3c, where stars from Figure 3a lying between 40–160 arcsec of the cluster center are displayed. The excess of blue HB (BHB) star candidates seen in Figure 2a is evident, indicating that they are spatially concentrated toward the

cluster center. The cluster’s red clump and red giant branch are better defined in this panel as well.

Figure 3d shows another effort to isolate NGC 6441 stars from the field. Here, we have statistically subtracted the CMD of off-cluster stars located between 40–160 arcsec of the frame center from the stars in Figure 3c. Before subtracting, we corrected for a 0.11 mag reddening difference between the fields (the off-cluster field has the higher reddening), which we estimated from the shift in color histograms of stars having values of the reddening-independent parameter  $V_{V-I} = V - 2.6(V - I)$  between 12.1 and 13.3 (Stanek et al. 1994). For each star in the off-cluster CMD, we removed from the on-cluster CMD the star nearest in color-magnitude space. Though the subtraction is over-aggressive for the faint stars, the brighter sequences (including the blue HB, red clump, and red giant branch) are more clearly shown.

The lack of faint, extremely blue HB stars in Figure 3c, relative to their abundance in the  $BV$  CMD of Rich et al. (1997), comes as a mild surprise. Even in CMDs where we relax the criteria on the photometric errors, these stars do not appear at  $V > 18$  mag. This suggests that these stars may be radially concentrated toward the cluster center, but we can not state this unequivocally without detailed completeness modelling. A simpler solution which lends itself to direct comparison with the Rich et al. (1997) data is to obtain deep, ground-based  $BV$  photometry of the cluster.

Does the prominence of the less extreme BHB (i.e., brighter than  $V \approx 18$  mag) vary with radial distance from the cluster center? Rich et al. (1997) found no evidence for a change in the number ratio of BHB to red clump stars with radius over their small *HST* field of view ( $\sim 100$  arcsec), and interpreted this as evidence against the production of BHB by dynamical effects. We can extend this search to larger radii using our  $VI$  photometry. For this purpose, we defined BHB stars as having  $16.8 < V < 18.0$  and  $0.3 < V - I < 0.8$  mag, and red clump stars as having  $13.6 < V_{V-I} < 13.9$  and  $1.30 < V - I < 1.56$  mag. We defined the number fraction

$$F = (N_{BHB,c} - N_{BHB,f}) / (N_{RC,c} - N_{RC,f})$$

where the  $f$  and  $c$  subscripts indicate stars counted from the cluster and field photometry sets, respectively. For stars in the radial annulus 50–100 arcsec, we obtained  $F = 0.054 \pm 0.012$ , while for radii of 100–240 arcsec, we obtained  $F = 0.027 \pm 0.008$ . The blue HB stars are a factor of two more prominent in the inner annulus. Such radial variations are often attributed to the effect of mass segregation, with more massive stars concentrating toward the cluster center. If true in this case, we are presented with the surprising situation where the BHB stars are *more* massive than their red clump counterparts. This contradicts the suggestion that the BHB stars are produced by tidally stripping normal RGB in the dense cluster core.

#### 4. Variable Stars

We used the Welch & Stetson (1993) variability index,  $I_{WS}$ , to characterize the likelihood that a given star is a variable. The value of  $I_{WS}$  is computed for each star from the individual  $V$  and  $I$  magnitudes and their errors. For a non-variable star,  $I_{WS}$  approaches zero as the number of observations becomes large, whereas for a variable,  $I_{WS}$  approaches a constant value. To minimize the effects of seeing and exposure depth (i.e., the blending of two nearby stars into a single measurable image as the seeing and/or signal-to-noise conditions worsen), we employed the frame groupings described in §2 and computed  $I_{WS}$  for each star detected more than four times in each group. Groups (a) and (b) were useful in detecting variable stars near the cluster ( $R < 1100$  pix), and groups (c) and (d) were useful outside  $R \approx 600$  pix<sup>4</sup>.

The morphology of the points in the ( $I_{WS}$ ,  $V$ ) plane led us to classify stars as probable variables ( $I_{WS} > 170$ ) and possible variables ( $50 < I_{WS} < 170$ ). When plotted on the cluster CMD, it became clear that three classes of variables are present: extremely red variables (Mira, semi-regular, and irregular variables, hereafter LPVs), blue variables (possible RR Lyrae stars), and a few other variables scattered around the CMD. We focused on these stars as follows: all stars with  $V - I > 2.4$  mag and  $I_{WS} > 50$  (LPV candidates), all stars with  $V - I < 1.4$  mag and  $I_{WS} > 50$  (RRL candidates), and all other stars with  $I_{WS} > 120$ . We enhanced our search for cluster RRL stars by supplementing the RRL candidates with stars in the subset  $V - I < 1.5$  mag,  $16.8 < V < 17.8$ , and  $30 < I_{WS} < 50$ . We produced analogous lists from the data in groups (b), (c), and (d), and merged them into a final list of 115 variable star candidates.

We then plotted the  $V$  and  $I$  magnitudes as a function of time for each candidate. The LPV candidates were characterized by constant or slowly-varying  $V$  and  $I$  magnitudes, with distinct jumps between the May and June data. Two candidates near the cluster center were sufficiently crowded, and their light curves scattered, that we could not unambiguously characterize them as LPVs; their positions and magnitudes are recorded in Table 5 (stars SV6 and SV7). The remaining LPV stars are considered in §4.2.

Among the 56 RRL candidates, 33 had time-magnitude plots which suggested that a close pair of non-variable stars in some frames had been resolved and in others was detected as a single star; when the photometry from the various frames was matched (based on position), the blended photometry was systematically brighter than the resolved photometry, and a large value of  $I_{WS}$  resulted. Inspection of the images almost always confirmed the blended-neighbor hypothesis. We discuss the remaining 23 candidates in detail in §4.3.

---

<sup>4</sup>An alternative approach would have been to develop a master list of star positions from the best seeing frames, and to measure magnitudes for all the stars in this list on each frame. In practice, the residuals of the fits used to transform the stellar coordinates from one frame to the next were large relative to the tolerance required for accurate PSF-fitting using fixed coordinates. However, the residuals were sufficiently small to enable reliable matching of stars from frame to frame.

Of the 16 variable star candidates scattered over the CMD, all but one were found to be false detections of critically-resolved, non-variable pairs. The single true variable has a color ( $V - I \approx 2.1$ ) consistent with an LPV near maximum light, so we have grouped it with the other LPV stars in Table 2 (V35). Clearly, the large number of critically-resolved stars in this dense stellar field presents a complication to the identification of variable stars, but one that is surmountable given careful attention.

#### 4.1. Previous Studies of Stellar Variability

The *Catalogue of Variable Stars in Globular Clusters* (Hogg 1973), as updated by Clement (1997), lists twelve variable stars in NGC 6441. No photometric or variable-type information is given. Stars V7 and V8 lie outside our field of view. Only variables V1, V6, and V19 were detected as variables in our study. Examination of the remaining stars' photometry showed that V2, V3, V5, and V10 are all LPVs, but were absent from enough frames due to saturation and other effects to sidestep detection. V4 showed no sign of variability in our observations, but at  $V - I = 2.84$ , is red enough to be an LPV (see §4.2). V11 and V12 are much fainter, bluer stars which Hesser & Hartwick (1976) suspected as being RR Lyrae stars; our photometry shows no sign of variability in these stars (see Table 5 and the Appendix).

#### 4.2. Long-Period Variable Stars

Data for the 31 LPV stars (i.e., stars which varied on timescales longer than a few days) found near NGC 6441 are presented in Table 2. The first column gives the variable star designation (in roughly decreasing value of the  $I_{WS}$  variability index). We name our newly-discovered variables V13, V14, etc. The second and third columns give the position of the star in the  $X$  and  $Y$  coordinate frame of Figure 1 (in units of pixels). The right ascension and declination offsets from the cluster center (in arc seconds, with positive values indicating East and North) can be computed from the pixel positions as follows,

$$\Delta\alpha = -0.396(X_{\text{pix}} - 1014), \quad \Delta\delta = -0.396(Y_{\text{pix}} - 1000)$$

The remaining columns give the magnitude-mean  $I$  magnitude ( $\bar{I}$ ), the mean color ( $\bar{V - I}$ ), and the number of observations ( $N$ ) during the May and June observing runs. In  $\sim 40\%$  of the stars, we observed a significant change in brightness or color during one or both observing runs. The previously identified LPVs not detected in our study (see §4.1) are included at the bottom of this table.

Clearly, the data here do not fully sample the LPVs' light cycles, and thus do not accurately represent the stars' mean photometric properties. Still, the locations of the stars on the CMD, shown in Figure 4, approximately represent these mean positions. Furthermore, the limited phase

coverage leads to LPV detection incompleteness; the observed  $V$  and  $I$  magnitude differences of some true LPVs (e.g., V4) were insufficient to result in  $I_{WS}$  values large enough to trigger detections. Finally, saturation and other image complications left some stars with too few observations to fulfill all the variability detection criteria. Thus, it is likely that many more of the stars with  $V - I > 2.4$  are LPVs, in particular faint, red LPVs near the cluster center.

### 4.3. RR Lyrae Variables and Eclipsing Binaries

In an effort to determine the types of variable stars present among the 23 blue variable star candidates discussed above, we attempted to find the period of each star and create the star's mean light curve. Classical period finding techniques such as Fourier transforms or Phase Dispersion Minimization perform poorly, if at all, when the data are sparse and irregularly spaced. We therefore developed the following new method.

In cases where a star's variable type is suspected (e.g., an RR Lyrae), it is possible to assume a period and fit the folded light curve with an appropriate template light curve. If the assumed period is near the true period, the scatter about the fitted template will be small. By folding the time-magnitude data by a sequence of periods typical of the variable type, and fitting the template and computing the scatter (or  $\chi^2$ ) at each period, one can easily identify  $\chi^2$  minima indicative of possible periods. This method is similar to that described by Stetson (1996).

In practice, we used the template-fitting procedure described in Layden (1998). We fit each star with three templates;  $V_3$  and  $V_4$  from Layden (1998, Table 4) are typical of RR $a$  and RR $b$  type variables, respectively, while a cosine curve was used to represent RR $c$  and contact binary LCs. We fit the templates over periods ranging from 0.2 to 1.0 days, increasing the period by 0.1% from one step to the next. If no suitable minima were found, we searched on the period interval 1–3 days. Periods longer than 3 days are evident in the time-magnitude plots. Since the templates are seldom a perfect match for the actual LCs, we refined the periods by folding the time-magnitude data by a sequence of periods near the  $\chi^2$  minimum, plotting the resulting LCs, and choosing the cleanest LC. This resulted in tighter LCs and improved periods.

We note that this technique should be applicable to any type of variable with a characteristic LC. Indeed, by including template LCs from a large number of variable types, it should be possible to determine both period *and* variable star type from the template giving the smallest  $\chi^2$  value.

Of the 23 blue variable candidates, we were able to determine periods for 11 RR Lyrae stars (V36–V46) and two contact binaries (V48 and V50). Light curves for two detached binaries (V49 and V51) and one long period star (V6, a Cepheid?) were obtained by examination of the time-magnitude plots. The  $V$  and  $I$  light curves of these 15 stars are presented in Figure 5. Possible periods were obtained for five additional stars (SV1–SV5, see Table 5). We were unable to determine with certainty whether these stars were low-amplitude RR Lyrae or contact eclipsing binaries (see Figure 6). We were unable to obtain periods or LCs for the remaining two blue

variable candidates, which we list in Table 5 as SV8 and SV9.

Table 3 lists the photometric properties of the 11 RR Lyrae stars. Columns include the location of the stars in the coordinate frame of Figure 1 ( $X_{\text{pix}}$  and  $Y_{\text{pix}}$ ), the period in days, the intensity-mean  $V$  and  $I$  magnitudes ( $\langle V \rangle$  and  $\langle I \rangle$ ), the  $V$ -band amplitude ( $\Delta V$ ), the mean color during the phase interval 0.5–0.8 ( $(V - I)_{\text{min}}$ ), and a brief comment. For several stars, a few discrepant data points were omitted from the computations, (e.g., V37), while for several other stars, only good-seeing data were used (e.g., V42 and V43). These data will prove useful in determining the nature of these unusual stars in the following section.

Table 4 reports the positions of the four eclipsing binaries from Figure 5, along with their periods,  $V$  and  $I$  band maxima and amplitudes, and a comment. Table 5 lists the positions, magnitude-mean  $V$  magnitudes and  $V - I$  colors of the uncertain and suspected variables, along with a brief comment.

The time series photometry for each of the variables is given in Table 6. The columns include the variable star name, the heliocentric Julian Date of mid-observation ( $HJD$ ), the  $V$ -band magnitude and its error ( $\sigma_V$ ), the  $I$ -band magnitude and its error ( $\sigma_I$ ), and a quality code ( $Q$ ) which corresponds to the symbols used in the light curves:  $Q = 1$  indicates a long exposure under good seeing conditions ( $\bullet$ ),  $Q = 2$  indicates a short exposure in good seeing ( $\circ$ ),  $Q = 3$  indicates a long exposure in poor seeing (solid triangle), and  $Q = 4$  indicates a short exposure in poor seeing ( $\triangle$ ). Figure 7 shows the finder charts for each variable star.

#### 4.4. Cluster Membership

The positions of the variable stars in the CMD and their radial locations with respect to the centroid of the cluster light provide useful information regarding the stars' membership in the cluster. Figure 4 shows the variable stars placed in the CMD, while Figure 8 shows the cumulative radial distributions of the stars in various classes. The squares in Figure 8 give the total sky-subtracted  $V$ -band photon counts inside the radius  $R$ , normalized by the amount at  $R = 440$  arcsec. The crosses give the analogous counts expected if a uniform stellar distribution were spread across the usable pixels of the CCD. The lines are the normalized cumulative radial distributions of various classes of stars, selected from the CMD as follows. Red clump stars (solid line) lie in the parallelogram bounded by  $13.6 < V_{V-I} < 13.9$  and  $1.3 < V - I < 1.56$ , blue HB stars (dotted line) lie in the rectangle  $16.8 < V < 17.6$  and  $0.3 < V - I < 0.9$ , while the LPV (long dash), RR Lyrae (short dash), and eclipsing binaries (dash-dot line) were taken from Tables 2, 3, and 4, respectively. The radial locations of the suspected variables in Table 5 are indicated along the top of the figure.

First, consider the four well-established eclipsing variables (Table 4). These stars are scattered about the CMD (Figure 4) and their location relative to the cluster is consistent with a uniform distribution across the CCD field (Figure 8). Thus, it is reasonable to assume that these stars are

members of the foreground stellar populations, probably the old disk (Rucinski 1997).

Next, consider the RR Lyrae stars from Table 3. Eight of these stars are clustered near  $(V - I, V) = (1.1, 17.3)$ , just blueward of the prominent cluster red clump, and just redward of the blue HB stars. Of these three classes of stars, the red clump stars are the least radially concentrated (Figure 8), as expected if a significant population of field red giants contributes to the counts. The BHB stars are more centrally concentrated, and the RR Lyrae stars seem even more so, though the number of stars involved is small and the expected background contamination varies between the three stellar classes. Note that all three of these distributions drop precipitously within 1 arcmin of the cluster center, indicating that our detection incompleteness increases at smaller radii, reaching 100% inside  $\sim 30$  arcsec. It seems clear that these eight RR Lyrae belong to the cluster.

Of the other three RR Lyrae from Table 3, V36 is almost certainly a foreground star. Its location 297 arcsec from the cluster, its position in the CMD just blueward of the bulge red clump, and its light curve parameters (see §5.1) are all consistent with it being a member of the Galactic bulge. The nature of V41 and V44 is less clear, and discussion of these stars is reserved for §5.3.

The LPV stars from Table 2 have a distribution in Figure 8 very similar to that of the star light between 1 and 4 arcmin. Inside 1 arcmin, incompleteness sets in, though not as quickly as for the fainter HB stars. Suspected variables SV6 and SV7 are probably cluster LPVs whose photometry has been compromised by stellar crowding. Thus, most of the LPVs in Table 2 probably belong to the cluster. In the CMD, most of the LPVs form a fairly tight, linear sequence running from  $(V - I, V) = (2.6, 15.6)$  to  $(5.0, 18.0)$ . A set of five LPVs appears to parallel this sequence  $\sim 0.8$  mag brighter. These five stars (V3, V5, V9, V30, and V31) have a cumulative radial distribution consistent with a uniform foreground population. Given that the distance modulus difference between the cluster and the bulge is  $\sim 0.8$  mag, based from the offset in  $V$  magnitudes of the red clumps and RRL stars, it seems reasonable to conclude that these five bright LPVs belong to the bulge, rather than the cluster.

The population of the two LPVs  $\sim 1.0$  mag fainter than the cluster LPV sequence is unclear. Their magnitudes and large radial distances from the cluster ( $R = 215$  arcsec for V25 and 322 arcsec for V28) suggest they are members of the background field. It is conceivable that they belong to the Sagittarius dwarf galaxy, but (i) the distance modulus between Sagittarius and the bulge is  $\sim 2.5$  mag (Sarajedini & Layden, 1995), 0.7 mag too large for the observed offset, and (ii) NGC 6441 is over 10 degrees from the nearest part of Sagittarius in the map of Ibata et al. (1997). Complete light curve coverage of these variables would enable estimates of their distances, while spectroscopy would indicate whether their radial velocities are consistent with an origin in the Galaxy or in Sagittarius.

Finally, we consider the variables of uncertain type from Table 5. Of these five stars, SV2, SV3, and SV5 lie in the clump of bona-fide cluster RRL in Figure 4, and so we tentatively consider them to be RRL as well. Their radial locations (Figure 8) are consistent with those of the other

RRL. While SV4 has the correct  $V$  magnitude, it is 0.3 mag bluer than the other RRL. Whether SV1 is a c-type RR Lyrae or a contact binary, its location in the CMD clearly indicates that it belongs to the foreground field.

## 5. Discussion

### 5.1. The Period-Amplitude Diagram

The Period-Amplitude (P-A, or Bailey) diagram is a useful, reddening-independent tool for comparing RR Lyrae variables. For typical RRL in the field and in metal-poor globular clusters, a star's position in this plane depends on its metallicity. In Figure 9, we show the metal-rich field ab-type RRL (periods and amplitudes from Bookmeyer et al. 1977, metallicities from Layden 1994). At a given amplitude, the more metal-rich stars have systematically shorter periods. The ab-type RRL in the globular cluster NGC 6171 (Dickens 1970;  $[Fe/H] = -1.04$ , Harris 1996) overlie the field RRL of similar metallicity, while that cluster's c-type RRL clump near  $(\log P, \Delta V) = (-0.5, 0.5)$ .

The RR Lyrae stars in NGC 6441 are systematically displaced to longer periods and smaller amplitudes. The bulge RRL V36 is marked by the large asterisk at  $\Delta V \approx 1.2$ , a position suggesting a metallicity of  $[Fe/H] = -1.0$  to  $-1.2$ , consistent with the distribution of metallicities in bulge RRL (Walker & Terndrup 1991). The large asterisks at lower amplitude mark the anomalously red variables V41 and V42. The open circles mark the suspected c-type RRL SV2, SV3, and SV5. The solid circles mark the remaining RRL in Table 3.

These results are consistent with the positions of the three previously-known long-period, metal-rich RRL: V9 in 47 Tuc (Carney et al. 1993), and V28 (ab-type) and V27 (c-type) in NGC 6388 (Silbermann et al. 1994). However, our data have more than tripled the number of members of this interesting sub-class of variable. Also, the positions of SV3, SV5, and perhaps SV2 support our interpretation that these stars are c-type RRL in NGC 6441.

### 5.2. Reddening

Using a variety of methods, Hesser & Hartwick (1976) estimated the interstellar reddening toward NGC 6441 to be  $E(B - V) = 0.46 \pm 0.15$  mag. They noted that, based on the appearance of the Palomar Sky Survey prints, "...the obscuration in the immediate vicinity of NGC 6441 is approximately uniform...". However, the large uncertainty they quote reflects the large range of solutions produced by the different techniques,  $0.23 \leq E(B - V) \leq 0.7$ . Furthermore, the large angular extent over which some of their estimates were obtained may produce deceptive results if significant patchiness exists on scales of several arcminutes or less. Zinn (1980) and Reed et al. (1988) obtained  $E(B - V) = 0.47$  and  $0.49$ , respectively, from integrated light measurements.

The RR Lyrae variables we have detected toward NGC 6441 provide an excellent opportunity to determine the reddening in a small region around the cluster. Mateo et al. (1995a) showed that the de-reddened  $V - I$  colors of typical RR Lyrae near minimum light (phases 0.5–0.8) is roughly constant. We determine  $(V - I)_0 = 0.57 \pm 0.02$  for the eight stars with  $[Fe/H] > -1.3$  listed by Mateo et al. (1995a). We use the apparent minimum-light colors of the 11 RRL in Table 3,  $(V - I)_{\min}$ , to determine the reddening,  $E(V - I)$  along each line of sight (see Table 7). These values are converted into  $E(B - V)$  and  $A_V$  using the relations of Dean et al. (1978).

Of these stars, only V36 is a “typical” RRL, judging from its position in the P-A diagram and its expected location in the Galactic bulge. Indeed, one could question whether the  $(V - I)_0$  colors of bulge RRL are the same as the local stars used to calibrate the relation. It is reassuring that V36 gives  $E(B - V) = 0.46 \pm 0.03$  mag, in excellent agreement with the existing reddening values.

Does the relationship work for the atypical, long-period variables in NGC 6441? Unfortunately,  $V - I$  colors do not exist for the two other known members of this class, V9 in 47 Tuc and V28 in NGC 6388. However, the data from Carney et al. (1993) on V9 indicates that the analogous relation employing  $(B - V)_{\min}$ , period, and metallicity (Blanco 1992 and references therein) *does* work, yielding  $E(B - V) = 0.03$ . For comparison, Harris’s (1996) compilation lists  $E(B - V) = 0.05$ . With this encouragement, and excluding the two anomalously red and bright stars V41 and V44, we find the mean  $E(B - V)$  of the nine RRL toward NGC 6441 to be 0.45 mag (0.05 mag rms). Again, our reddening estimate is in excellent agreement with the existing estimates.

The rms value is somewhat larger than expected from the estimated uncertainties ( $\sim 0.03$  mag for a single star). This suggests there may be some differential reddening across the face of the cluster. The extension of the cluster red clump along the reddening vector and the absence of a well-defined red giant branch provide similar evidence (see §3).

To search for further evidence of spatially-variable reddening, we considered individually the CMDs of stars lying in eight equal-sized sectors of an annulus with radius 40–100 arcsec centered on the cluster (the angles  $\alpha_1$  and  $\alpha_2$  in Table 7 define the bounds of each sector, and are measured counter-clockwise from a line radiating in the  $+x$  direction from the cluster center in Figure 1). For each CMD, we isolated the red clump stars using  $13.6 < V_{V-I} < 13.9$  and produced their generalized color histogram (see Figure 10). Several curves are substantially displaced towards redder colors, indicating the presence of differential reddening. Sector 4 is particularly noticeable. The median  $V - I$  color of each histogram ( $Med(V - I)_{13.9}^{13.6}$ ), and the number of stars involved ( $N_{\text{sec}}$ ), are shown in Table 7. The widths of the individual histograms are not drastically larger than the color width of the red clump in 47 Tuc ( $\sim 0.2$  mag, Armandroff 1988), suggesting that the effects of differential reddening within a given sector are small, though red giant branches in the CMDs are still noticeably broadened (especially in Sector 4). The small-scale peaks in the Figure 10 histograms are due to shot noise, indicating that further spatial segregation of the cluster is not warranted.

In an effort to recover the de-reddened CMD of the cluster, we corrected the differential reddening in the individual sectors to a representative mean ( $\langle Med(V - I)_{13.9}^{13.6} \rangle = 1.420$ , the average of Sectors 1, 2, 5 and 6), and then corrected the entire dataset for the average RRL reddening ( $\langle E(V - I) \rangle = 0.577$ , based on the RRL stars in or near those sectors). We assumed  $A_V = 2.6E(V - I)$ . The de-reddened CMD is shown in Figure 11. The principal sequences seem to have tightened up somewhat, compared with Figure 3c. However, the slope of the red clump stars persists, confirming the Rich et al. (1997) *HST* photometry. Sweigart & Catelan (1998) note that this intrinsic slope rules out older cluster age or extreme mass loss on the giant branch as causes of the extended blue HB seen in NGC 6441.

### 5.3. V41 and V44

The nature of the variables V41 and V44 is unclear. Their LCs suggest they are RR Lyrae stars, or possibly another class of pulsating variable. They are both  $\sim 0.7$  mag brighter, and  $\sim 0.3$  mag redder, than the other eight cluster RR Lyrae. Both are located close to the cluster center (63 and 57 arcsec, respectively), so are likely to be members.

One possibility is that they are Type II Cepheids belonging to the cluster. However, we searched for periods between 1 and 5 days and found no reasonable minima, and the time-magnitude plots indicate shorter period variations. Anomalous Cepheids have periods between 0.36 and 1.6 days, absolute magnitudes between 0.5 and 2 mag brighter than RRL, and colors comparable to RRL (Nemec et al. 1994). Based on the first two criteria, V41 and V44 could be anomalous Cepheids. However, both stars are significantly redder than the RRL in NGC 6441. Furthermore, most anomalous Cepheids are found in dwarf spheroidal galaxies, metal-poor systems with a component of younger stars ( $\leq 5$ –10 Gyr, Mateo et al. 1995b). Bono et al. (1997a) confirm theoretically that the minimum mass for the formation of anomalous Cepheids is  $\sim 1.8 M_\odot$  at  $[Fe/H] = -1.7$ , and this minimum increases quickly with increasing metal abundance. It seems unlikely that NGC 6441 possesses a population of stars young enough to produce HB stars of this mass. It may also be possible to produce anomalous Cepheids through binary star coalescence, but at the metallicity of NGC 6441, the mass limit appears incompatible with turnoff stars of globular cluster age ( $M \approx 0.8M_\odot$ ). Given these complications, and that we are not aware of the existence of any metal-rich examples of this type of variable, it seems unlikely that V41 and V44 are anomalous Cepheids.

Another possibility is that V41 and V44 are RR Lyrae stars in the foreground bulge. The similarity of their  $V$  magnitudes to that of V36 supports this idea, but their much redder  $V - I$  colors would require a large amount of differential reddening. The two stars *do* lie near each other, 21 arcsec apart in Sector 3; perhaps they lie behind a small, dense foreground dust cloud. To test this, we extracted a subset of the stars in Table 1 which lie within 20 arcsec of the stars' centroid, and plotted their CMD. It shows no displacement relative to the CMD of the other stars in Sector 3, nor to Figure 3c, indicating that heavy differential obscuration is *not* responsible for

the anomalous colors of these stars. Furthermore, the central location of V41 and V44 argues strongly for cluster membership. If they belong to the field, the probability of both variables lying inside 63 arcsec radius is  $4 \times 10^{-4}$ .

A third possibility is that V41 and V44 are cluster RRL whose photometry has been contaminated by another star. If the RRL components are typical of the other eight cluster RRL, then the contaminating stars must have  $V \approx 17.4$  and  $V - I \approx 1.6$ , roughly like those of cluster red clump stars. The positions of V41 and V44 in the Period-Amplitude diagram (Figure 9) are consistent with this interpretation. The observed amplitudes are small compared with the other RRL in NGC 6441 with the same period, but the amplitudes become consistent with these stars when corrected for the effect of the photometric companion just described: the  $V$ -band amplitude of V41 becomes  $\sim 0.7$  mag, and of V44 becomes  $\sim 1.2$  mag. Finally, the values of the “sharp” parameters produced by DAOPHOT are typical of stars of their brightness, indicating that the angular separations of the contaminating stars are small compared to the seeing disk. Perhaps V41 and V44 are members of physical binaries with red clump stars.

We conclude that V41 and V44 are probably RR Lyrae members of NGC 6441, but appear brighter and redder than the other cluster RRL because their photometry has been contaminated by the light of unresolved red clump companions. Images with higher spatial resolution and detailed spectroscopy may confirm this conclusion (unfortunately, V41 and V44 were just off the *HST* images of Rich et al. 1997).

#### 5.4. Light Curve Shapes

The light curves of “normal” c-type RR Lyrae in clusters and the field have a characteristic shape, not unlike a sine wave in which the region of maximum brightness has been skewed slightly toward smaller phases. That is, the phase interval of “rising light” between minimum and maximum brightness is shortened,  $\Delta\Phi_r < 0.5$ . Among the 31 c-type RRL in the *General Catalog of Variable Stars* (Khlopov 1985) with  $V$ -band photometry,  $\Delta\Phi_r$  ranges between 0.32 and 0.46, with a mean of 0.39 and rms of 0.04.

Figure 6 shows that the LC shapes of the c-type RRL in NGC 6441 depart somewhat from this norm. Their maxima appear skewed to longer periods, and  $\Delta\Phi_r > \sim 0.5$ . The minima may be uncharacteristically sharp as well, especially in the case of SV3. Clearly, better LCs (more observations with smaller errors) for more stars are required to verify this phenomenon. When the observations are confronted with stellar pulsation models (e.g., Bono et al. 1997b), this effect may prove to be a valuable tool for constraining the parameters responsible for bright, blue HB extensions in NGC 6441 and NGC 6388 (e.g., Sweigart & Catelan 1998). The light curve shapes of the ab-type RRL in NGC 6441 appear to fall within the range of shapes exhibited by “normal” ab-type RRL.

### 5.5. Comparison with Extended BHB Models

Rich et al. (1997) concluded that neither age nor dynamical effects, individually, could account for the extended blue HB in NGC 6441, though they could not rule out a combination of the two. Sweigart & Catelan (1998) used synthetic HB models to explore the effects of changing parameters which may produce blue HB extensions. They concur that neither age nor enhanced RGB mass loss produce the sloped HB, and hence luminous BHB extension, seen in NGC 6441. They considered three additional scenarios, (1) high initial helium abundance, (2) core rotation, which at the RGB tip allows both enhanced mass loss and formation of an over-massive core, and (3) envelope helium abundance enhancement from deep mixing during the RGB phase.

In their brief report, Sweigart & Catelan (1998) could not present detailed results of their models. We employ three means of comparing their models and *BV* synthetic CMDs with our *VI* photometry: (a) the number ratio of HB stars to RGB stars brighter than the mean RRL luminosity,  $R$ , (b) the pulsation characteristics of the RRL, and (c) general morphology of the stars along the HB.

Measuring the  $R$ -ratio in our photometry is complicated by the high degree of contamination by stars in the foreground and by stars on the cluster asymptotic giant branch (AGB). Using as a guide a field-subtracted version of Figure 11, we defined regions in which to count the number of BHB, red clump, and red giant stars. These regions are shown in Figure 11. We counted the number of stars in each region on the unsubtracted, de-reddened cluster CMD (Figure 11) and the equivalent de-reddened field CMD. The counts are given in Table 8. We add nine RRL to the BHB counts and ten LPV stars to the RGB counts. We used the luminosity functions of Bertelli et al. (1994;  $Z = 0.008$ ,  $Y = 0.25$ , Age = 14 Gyr) to estimate that 64% of the stars in the RGB region are first ascent red giants (36% are AGB stars). Combining the BHB and red clump counts, we obtain  $R = N_{\text{HB}}/N_{\text{RGB}} = 1.60 \pm 0.14$ , where the error is due solely to Poisson statistics. Systematic errors incurred by inappropriately defined counting regions are surely higher. If the counts in each region are uncertain by 25%, the systematic error on our estimate of  $R$  is 0.66. Even with this level of uncertainty, our counts strongly disfavor the high initial helium abundance scenarios of Sweigart & Catelan (1998). Their simulations with main sequence helium abundances of 0.38 and 0.43 produce sloping BHB extensions, but have  $R = 3.4$  and  $3.9$ , respectively, about  $3\sigma$  from our observed value<sup>5</sup>.

The pulsation properties of the cluster RRL stars provide other constraints on the Sweigart & Catelan (1998) models. Their Figure 3 shows the positions of their model BHB stars (helium mixing scenario with intermediate mass loss) in the temperature-period diagram. The dotted

<sup>5</sup>In fact, we have underestimated the RGB counts in this analysis. The faint boundary of the RGB region is usually defined as the bolometric magnitude equal to that of the RR Lyrae stars. However, this limit passes through the red clump stars. To avoid miscounts, we raised the faint boundary to that shown in Figure 11. Underestimating  $N_{\text{RGB}}$  results in overestimating  $R$ . The true value of  $R$  is therefore less than 1.60, and the disagreement with the model with high initial helium abundance is stronger.

region in our Figure 9 encloses those models. We transposed the region from the  $(\log T_{eff}, \log P)$  plane to the  $(\log P, \Delta V)$  plane using Equation 1 of Catelan (1998), which relates  $T_{eff}$  with  $[Fe/H]$  and the  $B$ -band amplitude,  $\Delta B$ . We converted from  $B$  to  $V$  amplitudes using the RRL in NGC 6171 (Dickens 1970):  $\Delta V = 0.72 \Delta B + 0.03$  (rms = 0.04) mag, and we assumed  $[Fe/H] = -0.53$  dex. Clearly, the model provides a reasonable, though not perfect, match to the RRL stars in NGC 6441, NGC 6388, and 47 Tuc. It will be interesting to compare the observations with the temperature-period predictions of the other scenarios.

Finally, we compare the overall appearance of our observed CMD with the synthetic CMDs of Sweigart & Catelan (1998, their Figure 2) for their various scenarios. The steep slope of our red clump and its relation to the BHB are best matched by the scenarios with core rotation and helium-mixing, and moderate mass loss on the RGB (see their Figures 2c and 2e). Given the uncertainties introduced by differential reddening, foreground confusion, and by comparing the observed  $VI$  CMD with the synthetic  $BV$  CMD, we can not make a more quantitative statement at this time.

We can provide a measurement of the distribution of stars along the HB which may prove useful in constraining future synthetic HB models, and in comparing the HB of NGC 6441 with those of other globulars. The usual statistic is  $(B - R)/(B + V + R)$ , where  $B$  and  $R$  are the numbers of HB stars on the blue and red sides of the instability strip, and  $V$  is the number of RRL variables. We adopt the same CMD regions as above except that the section of the BHB region redward of  $(V - I)_0 = 0.49$  (the mean de-reddened mag of the RRL in Table 7, see counts in row labeled “RHB” of Table 8) is now added to the red clump counts to produce  $R$ . Subtracting the counts in the off-cluster CMD from those in the on-cluster CMD, we obtain  $B = 45 \pm 10$ ,  $V = 9 \pm 3$ , and  $R = 648 \pm 29$  stars, so  $(B - R)/(B + V + R) = -0.86 \pm 0.03$  (Poisson)  $\pm 0.04$  (systematic). The HB is predominantly red, and only  $\sim 17\%$  of HB stars are in the blue extension.

It is tempting to use our photometry to measure the distance to NGC 6441. However, the long periods observed for its RRL suggest that they are more luminous than typical RRL, so the absolute magnitudes usually assumed for those stars may be inappropriate. Moreover, the different models presented by Sweigart & Catelan (1998, their Figure 2) have absolute magnitudes near the instability strip which range between 0.35 and 0.75 mag (we have omitted the high initial helium scenarios). The absolute magnitudes of the red clumps present a smaller range of 0.80–0.95 mag. Combined with a de-reddened apparent red clump magnitude of  $V_0 = 15.94 \pm 0.02$  mag from Figure 11, we find that NGC 6441 lies between 10.0 and 10.7 kpc from the Sun, on the far side of the Galactic bulge.

## 6. Summary and Conclusions

We present the first ground-based CCD photometry of the metal-rich globular cluster NGC 6441. Our  $VI$  color-magnitude diagram shows that the extended blue horizontal branch discovered

by Rich et al. (1997) using the *Hubble Space Telescope* exists even at large radii from the cluster center. Such hot HB stars are not expected in a cluster of this metallicity. Furthermore, over the radial range 50–240 arcsec, the blue BHB stars are more concentrated toward the cluster center than the red clump stars. If this effect is due to mass segregation, it implies that the BHB stars are more massive than their red clump counterparts, in contradiction with the hypothesis that BHB are produced by tidal stripping of red giants in the dense cluster core. Similarly, the intrinsic slope of the HB and red clump can not be explained by simple models involving old age or excessive mass loss (Sweigart & Catelan 1998).

Our time-series photometry enabled us to detect a large number of variable stars. We increased the number of red, long-period variables from nine to 32. We argue that five are members of the foreground bulge and that two are members of the background field, or possibly the Sagittarius dwarf galaxy. The remaining 25 are members of NGC 6441. We confirm the variability of V6, which may be a foreground Cepheid. Long-term monitoring of these variables is encouraged.

We also discovered 11 ab-type RR Lyrae variables, along with several probable c-type RRL. Based on their radial distances from the cluster center and positions in the CMD, we argue that eight of the ab-type RRL and 2–3 of the c-type RRL are members of NGC 6441. One RRL belongs to the foreground bulge, and two appear anomalously bright and red. We suspect the latter are photometric blends between cluster RRL and red clump stars, and note that they could be physical binaries. We also discovered four eclipsing binary stars in the foreground field, and several stars which we could not classify with certainty.

We present a method for determining variable star periods in which the data are folded by a sequence of periods, and at each period, are fit with a set of light curve templates. The  $\chi^2$  of the fits are then plotted as a function of the employed periods. Minima in this plot indicate probable periods.

Using this method, we determined periods for the RRL, and produced mean light curves in  $V$  and  $I$ . The 8–11 RRL in NGC 6441 have periods that are systematically longer than field RRL of comparable metallicity. RRL in the metal-rich globulars 47 Tuc (V9) and NGC 6388 (V27 and V28) have similar properties. Thus, a new sub-class of RRL appears to be emerging.

Using the observed  $V - I$  colors of the RRL at minimum light, we determined the reddening toward NGC 6441 to be  $E(B - V) = 0.45 \pm 0.03$  mag. Two points suggest that these long-period RRL have the same  $(V - I)_0$  colors as the “normal” RRL, (a) we obtain  $E(B - V) = 0.46$  mag from the bulge variable V36, and (b) the analogous relation for  $(B - V)_0$  at minimum light works for the long-period RRL V9 in 47 Tuc.

Evidence for small changes in the amount of reddening across the face of the cluster come from the star-to-star dispersion in the RRL  $E(B - V)$  values, and from differential shifts along the reddening vector of CMDs generated from small regions around the cluster. The South-East portion of the cluster has  $E(B - V) \approx 0.06$  mag higher than the rest of the cluster, though there

is evidence for patchy reddening on a scale of several arcmin or less.

We employ a differentially de-reddened color-magnitude diagram to count stars in various regions along the horizontal and red giant branches. We find the ratio of HB stars to red giants to be  $R = 1.6 \pm 0.7$ . About 17% of the HB stars lie blueward of the red clump, and  $(B - R)/(B + V + R) = -0.86 \pm 0.04$ , indicating a predominantly red HB.

The properties of the RRL and blue HB stars in NGC 6441 may help to determine which physical characteristics (e.g., age, helium abundance, core rotation, etc.) are responsible for the stars' unexpectedly high surface temperatures. As noted by Sweigart & Catelan (1998), the intrinsic slope of the HB, and in particular of the red clump, can not be produced by standard models invoking extreme cluster age or red giant branch mass loss. Similarly, our measurement of the HB-to-giant star ratio argues strongly against the Sweigart & Catelan (1998) model predictions for a scenario which involves high initial helium abundance. In contrast, the observed periods and amplitudes of our RRL are in reasonable agreement with their model predictions for a scenario in which the helium abundance in the atmosphere has been enhanced through rotational mixing. However, the results of the Sweigart & Catelan (1998) models appear to be rather sensitive to the assumed mass loss parameters (mean and distribution), which are at present poorly constrained by either observation or theory. Thus, it remains unclear whether the existing observations can isolate a unique set of physical parameters which explain the production of the extended blue HB.

We note one additional piece of observational evidence which may be brought to bear on this problem. The shapes of the c-type RRL light curves in NGC 6441 appear to differ significantly from their "normal" counterparts. They have longer phase intervals between minimum and maximum light, and the minima appear to be sharper. Perhaps by adjusting the physical parameters in stellar pulsation models (e.g., Bono et al. 1997b), similar light curves can be produced. If so, the intersection of plausible parameters from evolution and pulsation theory could further isolate the physical differences between "normal" clusters and those like NGC 6441. We encourage additional work on this problem both from the theoretical and observational perspectives.

We thank Márcio Catelan, Mario Mateo, Ata Sarajedini, and Horace Smith for helpful comments and suggestions. Support for this work was provided by NASA through Hubble Fellowship grant HF-01082.01-96A awarded by the Space Telescope Science Institute, which is operated by the Association of Universities for Research in Astronomy, Inc., for NASA under contract NAS 5-26555. Support was also provided by the National Science and Engineering Council of Canada through a grant to D.L.W.

## Appendix: Notes on Individual Variable Stars

**V01–V12:** Variable stars listed in the Hogg (1973) catalog (Clement 1997).

**V11 and V12:** Hesser & Hartwick (1976) identified these stars as possible RR Lyrae variables

(RRL). We obtained an rms scatter about the mean values in Table 5 of 0.03 mag in  $V$  and  $\sim 0.08$  mag in  $I$  for both candidates. Their  $I_{WS}$  variability indices are 0.0 and 3.2, respectively. Our data thus show no sign of variability in these stars. Indeed, they are  $> 0.2$  mag bluer than the *bona fide* RRL stars we have discovered (see Figure 4).

**SV1:** definitely variable, but the class of variable is uncertain. The data fold with minimal scatter at  $P = 0.3239$  days to produce the light curve (LC) of a c-type RRL, and at  $P = 0.6472$  days to produce the LC of a contact eclipsing binary. The star is  $\sim 0.8$  mag brighter than the member RRL.

**SV2:** definitely variable, but the class of variable is uncertain. The data fold with minimal scatter at  $P = 0.5612$  days to produce an RRL LC, and at  $P = 1.122$  days to produce the LC of a contact eclipsing binary. The RRL LC is too sharp at the extrema for a typical RRc, and the rise-time is too long for a typical RRab. However, the star falls among the other cluster RRL in the CMD.

**SV3:** definitely variable, but the variability class is uncertain. The data fold well at  $P = 0.9016$  days, yielding a contact eclipsing binary. A less convincing fold is achieved with  $P = 0.4508$  days to produce an RRc LC, but the minimum is too sharp and the maximum is skewed to late phases. The star's position in Figure 4 suggests it is an RRL member of NGC 6441.

**SV4:** definitely variable, but the variability class is uncertain. The  $V$ -band data fold well with  $P = 0.3167$  days, yielding an RRc LC, though the  $I$ -band curve has significant scatter. A period of  $P = 0.4814$  days yields a contact eclipsing binary with an eccentric orbit. The color is 0.3 mag bluer than the *bona fide* cluster RRL.

**SV5:** definitely variable, but the variability class is uncertain. The data fold well with  $P = 0.3615$  days, yielding an RRc LC, though the  $I$ -band curve has significant scatter. A period of  $P = 0.7230$  days yields a contact eclipsing binary with considerable asymmetry. The star's position in Figure 4 suggests it is an RRL member of NGC 6441.

## REFERENCES

Armandroff, T.E. 1988, AJ, 96, 588  
Bertelli, G., Bressan, A., Chiosi, C., Fagotto, F., & Nasi, E. 1994, A&A, 106, 275  
Blanco, V.M. 1992, AJ, 104, 734  
Bono, G., Caputo, F., Santolamazza, P., Cassisi, S., & Piersimoni, A. 1997a, AJ, 113, 2209  
Bono, G., Caputo, F., Cassisi, S., Incerpi, R., & Marconi, M. 1997b, ApJ, 483, 811  
Bookmeyer, B.B., Fitch, W.S., Lee, T.A., Wisniewski, W.Z. & Johnson, H.L. 1977, Rev. Mex. Astron. Astrofis., 2, 235  
Carney, B.W., Storm, J., & Williams, C. 1993, PASP, 105, 294  
Catelan, M. 1998, ApJ, 495, L81

Clement, C. 1997, <http://www.astro.utoronto.ca/~cclement/papers.html#catalogue>

Dean, J.F., Warren, P.R., & Cousins, A.W.J. 1978, MNRAS, 183, 569

Dickens, R.J. 1970, ApJS, 22, 249

Dorman, B. 1992, ApJS, 81, 221

Harris, W.E. 1996, AJ, 112, 1487 (1997 revision)

Hesser, J.E. & Hartwick, F.D.A. 1976, ApJ, 203, 97

Hodder, P.J.C., Nemec, J.M., Richer, H.B., Fahlman, G.G. 1992, AJ, 103, 460

Hogg, H.S. 1973 Publ. of the David Dunlap Observatory, Volume 3, No. 6

Ibata, R.A., Wyse, R.F.G., Gilmore, G., Irwin, M.J., & Suntzeff, N.B. 1997, AJ, 113, 634

Kholopov, P.N. 1985, General Catalog of Variable Stars, 4th ed. Nauka, Moscow

Landolt, A.U. 1992, AJ, 104, 340

Layden, A.C. 1994, AJ, 108, 1016

Layden, A.C. 1995a, AJ, 110, 2288

Layden, A.C. 1995b, AJ, 110, 2312

Layden, A.C. 1998, AJ, 115, 193

Lee, Y.-W., Demarque, P., & Zinn, R. 1990, ApJ, 350, 155

Liebert, J., Saffer, R.A., & Green, E.M. 1994, AJ, 107, 1408

Mateo, M., Udalski, A., Szymański, M., Kalużny, J., Kubiak, M., & Krzeminski, W. 1995a, AJ, 109, 588

Mateo, M., Fischer, P., & Krzeminski, W. 1995b, AJ, 110, 2166

Nemec, J., Nemec, A.F. Linnel, & Lutz, T.E. 1994, AJ, 108, 222

Preston, G.W. 1959, ApJ, 130, 507

Reed, B.C., Hesser, J.E., & Shawl, S.J. 1988, PASP, 100, 545

Rich, R.M., Sosin, C., Djorgovski, S.G., Piotto, G., King, I.R., Renzini, A., Phinney, E.S., Dorman, B., Liebert, J., & Meylan, G. 1997, ApJ, 484, L25

Rucinski, S.M. 1997, AJ, 113, 407

Sarajedini, A. & Layden, A.C. 1995, AJ, 109, 1086

Schechter, P., Mateo, M., & Saha, A. 1993, PASP, 105, 1342

Silbermann, N.A., Smith, H.A., Bolte, M. & Hazen, M.L. 1994, AJ, 107, 1764

Stanek, K.Z., Mateo, M., Udalski, A., Szymański, M., Kalużny, J., & Kubiak, M. 1994, ApJ, 429, L73

Stetson, P.B. 1994, PASP, 106, 250

Stetson, P.B. 1996, PASP, 108, 851  
Suntzeff, N.B., Kinman, T.D., & Kraft, R.P. ApJ, 367, 528  
Sweigart, A.V. & Catelan, M. 1998, ApJ, 501, L63  
Walker, A.R. & Terndrup, D.M. 1991, ApJ, 378, 119  
Welch, D.L. & Stetson, P.B. 1993, AJ, 105, 1813  
Zinn, R.J. 1980, ApJS, 42, 19

Table 1. Photometry of 16,011 Stars toward NGC 6441<sup>a</sup>

ID	$X_{\text{pix}}$	$Y_{\text{pix}}$	$V$	$\sigma_V$	$V - I$	$\sigma_{V-I}$
1	1267.64	-27.67	17.001	0.169	1.071	0.192
2	1336.58	-25.93	18.611	0.043	1.150	0.059
3	949.77	-25.65	17.553	0.151	1.567	0.171
4	1225.50	-25.00	18.059	0.021	1.206	0.030
5	1216.89	-24.55	18.799	0.041	1.135	0.069
6	901.32	-24.13	18.519	0.046	0.966	0.057
7	1327.34	-23.72	18.794	0.026	1.306	0.040

<sup>a</sup>Table 1 is presented in its entirety in the electronic edition of the Astronomical Journal. A portion is shown here for guidance regarding its form and content.

Table 2. Mean Photometry of Long Period Variable Stars

Star	$X_{\text{pix}}$	$Y_{\text{pix}}$	$\bar{I}_{\text{May}}$	$\bar{V} - \bar{I}_{\text{May}}$	$N_{\text{May}}$	$\bar{I}_{\text{Jun}}$	$\bar{V} - \bar{I}_{\text{Jun}}$	$N_{\text{Jun}}$
V13	1005	1185	12.98	3.49	5	12.59	3.05	18
V1 <sup>a</sup>	890	1112	13.76	4.97	6	12.85	4.20	17
V14	432	1183	12.89	2.70	5	13.27	3.17	20
V15	1156	1609	13.03	3.85	5	12.79	3.54	18
V16	1360	1147	13.16	3.65	5	12.90	3.12	18
V17	1182	937	13.19	2.88	5	13.43	3.05	19
V18	1463	49	12.78	3.90	5	13.04	4.09	19
V19	1065	1729	13.32	6.60	4	12.83	6.28	13
V20	477	1510	13.03	2.70	5	13.29	2.95	21
V21	1423	1401	13.02	4.53	5	12.81	4.39	17
V22	1268	1076	12.95	2.95	5	12.86	2.82	16
V23	979	1129	12.80	3.46	5	12.68	3.29	16
V24	480	962	13.07	3.06	5	13.17	3.19	17
V25	1431	1347	14.68	4.10	7	14.44	4.18	19
V26	1271	747	12.76	3.75	5	12.67	3.54	17
V27	823	396	12.98	3.02	5	12.93	2.97	17
V28	1092	190	14.33	2.44	7	14.29	2.37	21
V9 <sup>a</sup>	1073	1119	12.52	2.84	3	12.23	2.53	12
V29	1486	501	12.46	4.80	3	12.81	4.97	17
V30	354	658	12.38	3.08	3	12.26	2.93	12
V31	804	1581	12.14	3.02	3	12.25	3.12	12
V32	1062	1045	12.94	2.76	3	12.87	2.64	12
V33	936	986	13.00	2.56	5	13.15	2.70	13
V34	601	1580	13.31	3.26	4	13.23	3.14	19
V35	877	1017	13.52	2.19	5	13.39	2.11	19
V6 <sup>a</sup>	933	877	13.56	1.66	5	12.79	1.40	18
V2 <sup>a</sup>	918	938	12.09	2.70	3	13.32	4.25	4
V3 <sup>a</sup>	124	1212	11.60	3.49	3	12.37	4.74	12
V4 <sup>a</sup>	853	1440	13.00	2.88	5	13.00	2.90	18
V5 <sup>a</sup>	504	425	12.29	3.93	3	11.54	2.98	4
V10 <sup>a</sup>	819	1149	12.72	3.03	4	12.92	3.39	18

<sup>a</sup>see comment in Appendix.

Table 3. Photometry of RR Lyrae Variables

Star	$X_{\text{pix}}$	$Y_{\text{pix}}$	Period	$\langle V \rangle$	$\langle I \rangle$	$\Delta V$	$(V - I)_{\text{min}}$	Comment
V36	1703	1299	0.5078	16.54	15.50	1.16	1.16	
V37	926	705	0.6132	17.38	16.41	1.04	1.10	
V38	994	605	0.7347	17.35	16.33	0.76	1.10	
V39	716	847	0.8330	17.53	16.36	0.72	1.28	
V40	1088	1139	0.6490	17.22	16.21	1.11	1.18	
V41	923	1131	0.7345	16.65	15.26	0.38	1.46	see Appendix
V42	1011	765	0.8140	17.39	16.33	0.57	1.14	
V43	897	861	0.7730	17.38	16.34	0.52	1.10	
V44	975	1138	0.6090	16.58	15.23	0.64	1.45	see Appendix
V45	1179	1339	0.5028	17.15	16.11	0.73	1.09	
V46	1377	1198	0.9050	17.31	16.18	0.42	1.18	

Table 4. Photometry of Eclipsing Variables

Star	$X_{\text{pix}}$	$Y_{\text{pix}}$	Period	$V_{\text{max}}$	$I_{\text{max}}$	$\Delta V$	$\Delta I$	Comment
V47	836	1765	0.703	16.20	15.02	1.47	1.10	detatched
V48	158	1171	0.6674	15.23	14.22	0.32	0.28	contact
V49	365	768	1.010	16.52	15.45	0.36	0.20	detatched?
V50	838	1410	0.4335	17.85	16.55	0.55	0.55	contact?

Table 5. Photometry of Suspected Variable Stars

Star	$X_{\text{pix}}$	$Y_{\text{pix}}$	$\overline{V}$	$\overline{V - I}$	Comment
SV1	1364	1501	15.81	0.99	see Appendix
SV2	536	1057	17.22	1.03	see Appendix
SV3	580	1244	17.25	1.07	see Appendix
SV4	1268	1129	17.24	0.72	see Appendix
SV5	912	796	17.37	0.97	see Appendix
SV6	1062	940	16.89	2.59	crowded, LPV?
SV7	1034	969	15.13	2.49	crowded, LPV?
SV8	643	563	17.21	1.18	blended image, RR Lyrae?
SV9	1359	93	17.10	1.17	blended image, eclipsing binary?
V11	1120	755	17.86	0.48	non-variable, see Appendix
V12	1123	867	17.29	0.69	non-variable, see Appendix

Table 6. Time Series Photometry of Variable Stars<sup>a</sup>

Star	<i>HJD</i>	<i>V</i>	$\sigma_V$	<i>I</i>	$\sigma_{V-I}$	<i>Q</i> <sup>b</sup>
V1	258.6055	17.231	0.010	12.962	0.005	3
V1	258.6006	17.195	0.021	12.901	0.004	4
V1	258.8444	17.201	0.016	12.920	0.005	2
V1	258.8511	17.164	0.010	12.909	0.004	1
V1	259.5721	17.142	0.013	12.906	0.005	4
V1	225.6801	18.649	0.056	13.787	0.012	2
V1	260.7804	17.155	0.024	12.855	0.011	2
V1	260.7867	17.098	0.015	12.882	0.011	1
V1	226.6869	18.869	0.094	13.775	0.010	2
V1	226.6934	18.738	0.039	13.744	0.008	1
V1	262.5531	17.005	0.018	12.837	0.006	2
V1	262.5592	16.995	0.011	12.836	0.003	3
V1	262.7993	17.003	0.015	12.811	0.012	4
V1	262.8059	17.027	0.012	12.828	0.010	3
V1	227.6111	18.766	0.044	13.750	0.007	1
V1	263.5229	16.959	0.020	12.838	0.008	2
V1	227.8237	18.700	0.128	13.766	0.009	2
V1	227.8560	18.629	0.045	13.722	0.009	1
V1	263.7489	16.927	0.020	12.794	0.009	2
V1	263.8582	16.928	0.020	12.814	0.006	4
V1	263.8647	17.030	0.030	12.797	0.005	3
V1	264.4933	16.948	0.027	12.832	0.004	4
V1	264.4995	16.969	0.017	12.814	0.004	3
V1	265.8469	17.371	0.063	12.847	0.007	3
V1	266.7073	16.844	0.021	12.785	0.010	4
V2	258.8444	17.352	0.033	13.217	0.009	2
V2	225.6801	14.754	0.017	12.078	0.012	2
V2	260.7804	17.512	0.034	13.300	0.012	2

<sup>a</sup>Table 6 is presented in its entirety in the electronic edition of the Astronomical Journal. A portion is shown here for guidance regarding its form and content.

<sup>b</sup>Quality Code, *Q*. See §4.3 for definition.

Table 7. Reddening Toward NGC 6441

Sector	$\alpha_1^a$	$\alpha_2^a$	$Med(V - I)_{13.9}^{13.6}$	$N_{\text{sec}}$	RR Lyr	$E(V - I)$	$E(B - V)$
1	0	45	1.391	64	V36 <sup>b</sup>	0.588	0.456
					V46 <sup>b</sup>	0.612	0.474
2	45	90	1.429	63	V40	0.604	0.468
					V45	0.516	0.400
3	90	135	1.472	59	V41	0.884	0.683
					V44	0.874	0.676
4	135	180	1.524	95	-		
5	180	225	1.460	82	V39	0.707	0.548
6	225	270	1.401	79	V37	0.529	0.410
					V38	0.531	0.412
					V42	0.572	0.444
					V43	0.532	0.413
7	270	315	1.409	92	-		
8	315	360	1.393	90	-		

<sup>a</sup>These angles (in degrees) define the sector boundaries, see §5.2.

<sup>b</sup>V36 and V46 lie outside Sector 1, at radii of 300 and 165 arsec, respectively.

Table 8. Star Counts in NGC 6441

Region <sup>a</sup>	Cluster	Field
BHB	175	83
RRL	9	0
RC	642	41
RGB	918	238
LPV	10	0
RHB <sup>b</sup>	107	60

<sup>a</sup>CMD regions for BHB, RC, and RGB counts are defined in Fig. 11.

<sup>b</sup>Red HB region is the BHB region redward of  $(V - I)_0 = 0.49$  mag.

Fig. 1.— A 30 sec exposure image of NGC 6441 in the  $V$ -band. North is down and East is to the left. The field is 13.5' across. Pixel coordinates range from  $(X, Y) = (1, 1)$  at the lower-left to  $(2048, 2048)$  at the upper right, with the cluster center lying at  $(1014, 1000)$ .

Fig. 2.— Color-magnitude diagrams of stars toward (a) NGC 6441, and (b) a field centered 13.3' North of the cluster. In both panels, only stars with small errors ( $\sigma_V < 0.050$  mag and  $\sigma_{V-I} < 0.071$  mag) are shown. In (a), only stars lying within 440" of the cluster center are shown, while in (b) only stars within 400" are shown. The line segment represents the reddening vector ( $A_V = 1.0$  mag).

Fig. 3.— Color-magnitude diagrams for stars with moderate errors ( $\sigma_V < 0.10$  mag and  $\sigma_{V-I} < 0.14$  mag) and located (a) within 440" of NGC 6441, (b) within 400" of the center of the adjacent field, (c) between 40 and 160" of NGC 6441. In (d), the points in (c) are shown after the statistical subtraction of the CMD generated from off-cluster stars located in the same radial zone.

Fig. 4.— The NGC 6441 color-magnitude diagram from Fig 3a with the variable stars marked as follows: long-period variables from Table 2 (*squares*); RR Lyrae stars from Table 3 ( $\bullet$ ); eclipsing binaries from Table 4 ( $\triangle$ ); variables of uncertain class (SV1–SV5) from Table 5 ( $*$ ); and the remaining suspected variables from Table 5 ( $\times$ ).

Fig. 7.— Finder charts for the variable stars. Each image is 20" square, and is oriented with North at the top and East to the left. For the LPVs (V1–V35 plus SV6 and SV7),  $I$ -band images are used, while  $V$ -band images are used for all other stars.

Fig. 11.— The differentially de-reddened color-magnitude diagram of NGC 6441. Variable stars are indicated as follows: long period variables (*filled square*), ab-type RRL ( $\bullet$ ), suspected c-type RRL ( $*$ ). The dotted boxes define the regions used to count blue HB stars (BHB), red clump stars (RC), and red giant branch stars (RGB) in Sec. 5.5.

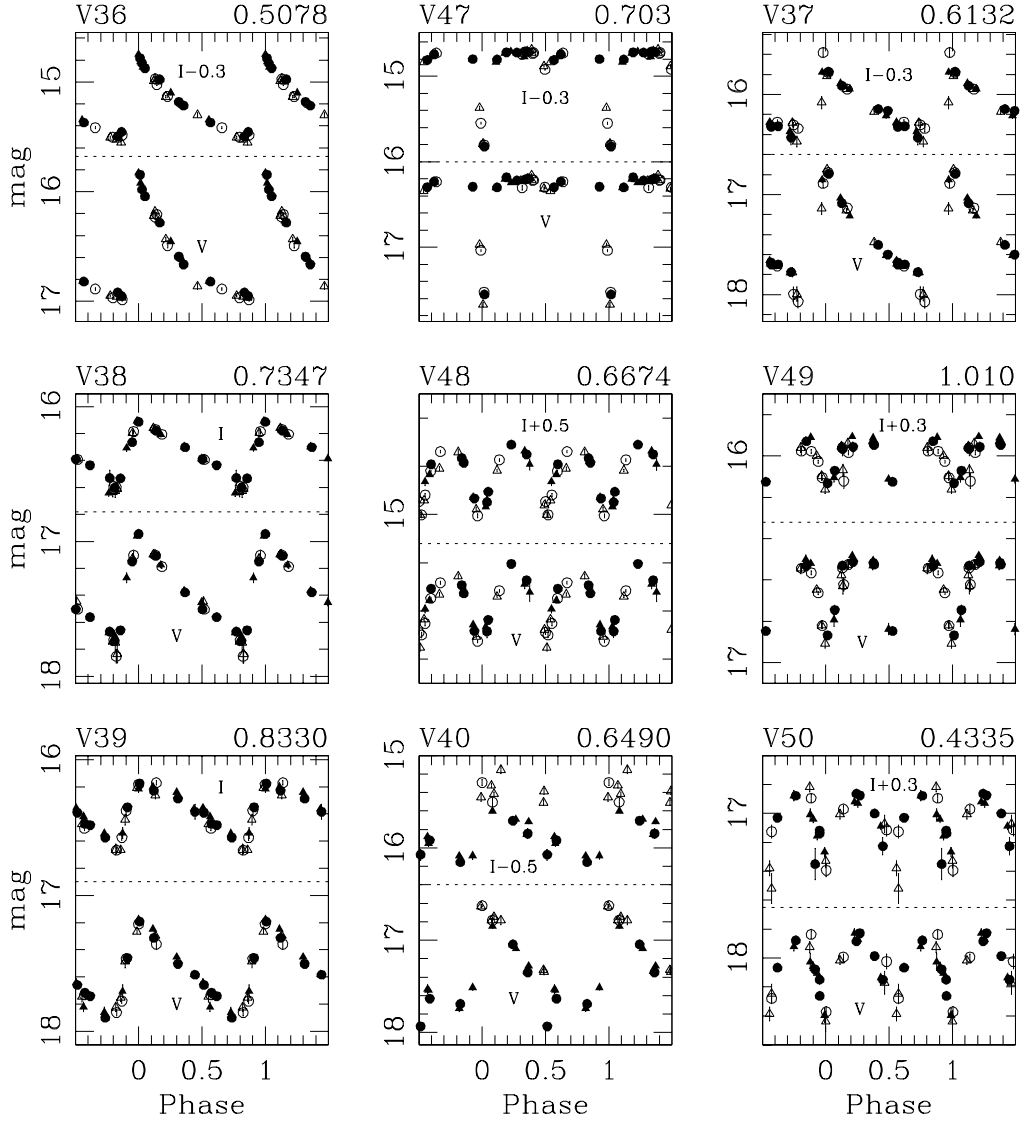


Fig. 5.— Mean light curves for the blue variable candidates which yielded clear periods. Each panel shows the  $V$  (lower curve) and  $I$  (upper curve, in some panels offset vertically by the indicated amount for convenience of display) light curve for the indicated star and period. In all panels, the minor tick marks indicate intervals of 0.2 mag. See Figure 12 for additional light curves.

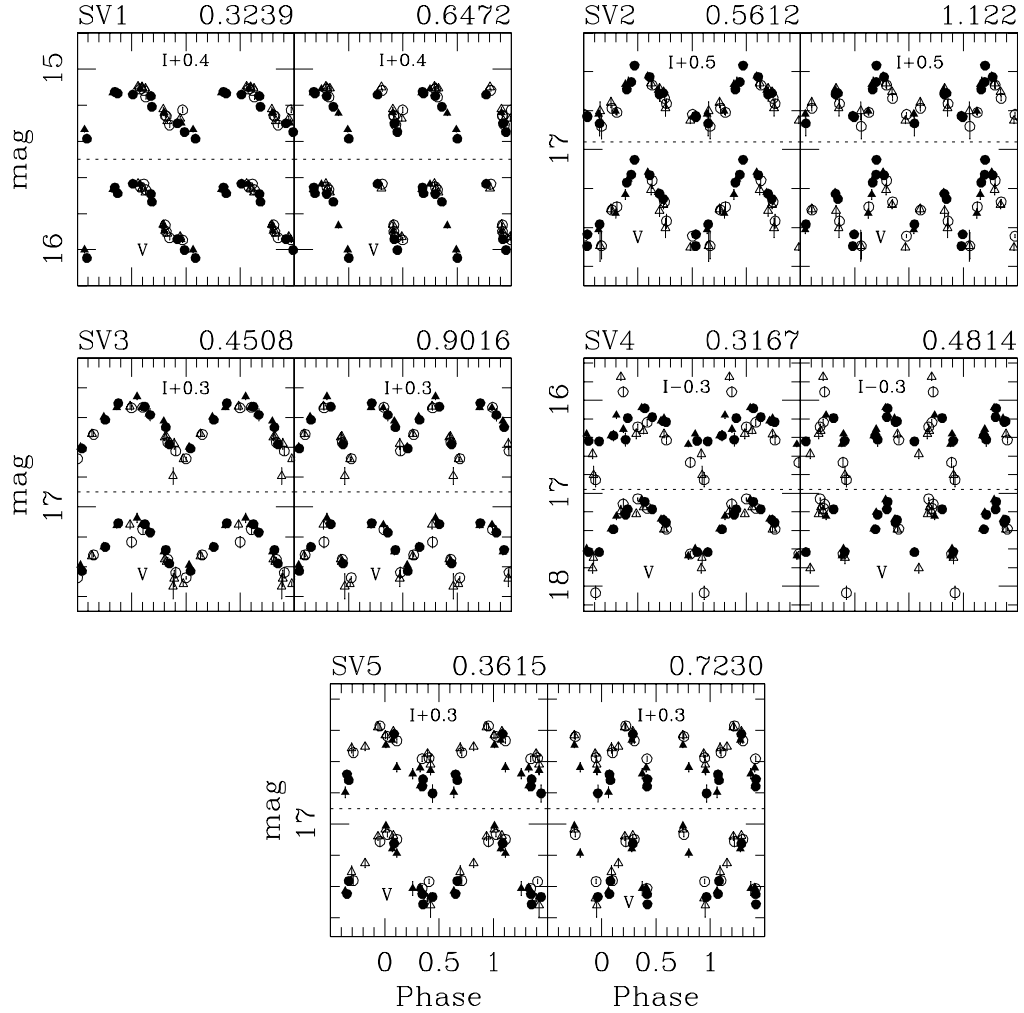


Fig. 6.— Mean light curves for the blue variable candidates which yielded two possible periods. In each panel, the left-most set of light curves ( $V$  below;  $I$  above, possibly shifted vertically) employs the shorter period and has the characteristics of a c-type RR Lyrae, while the right-most set employs the longer period, and resembles a contact binary.

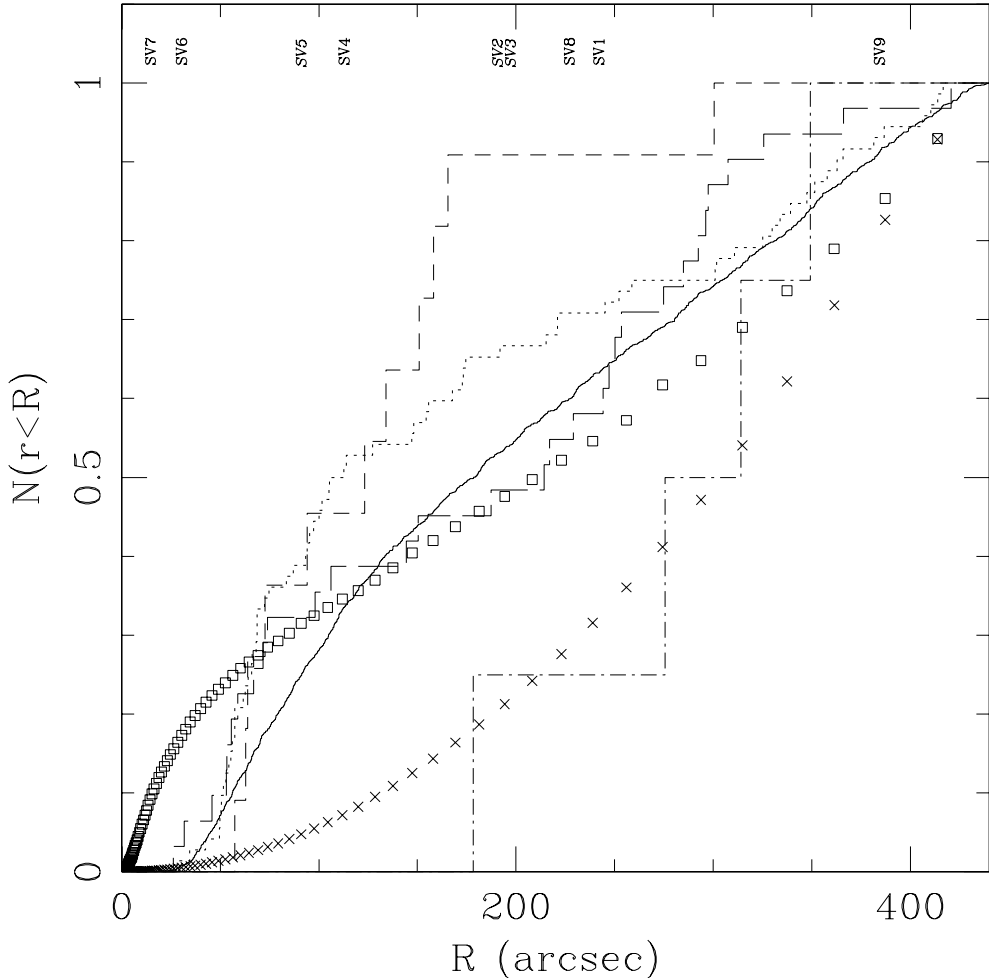


Fig. 8.— The cumulative radial distributions of stars of various class, normalized to the total number inside  $440''$  radius. *Squares*:  $V$ -band light distribution (sky subtracted, in intensity units). *Crosses*: model light distribution for stars uniformly distributed across the usable CCD pixels. *Solid line*: red clump stars. *Dotted line*: blue HB stars. *Short dashed line*: RR Lyrae stars. *Long dashed line*: LPV stars. *Dash-dot line*: eclipsing binaries. The radial locations of the suspected variable stars are marked along the top, with the probable RR Lyrae stars in *italics*.

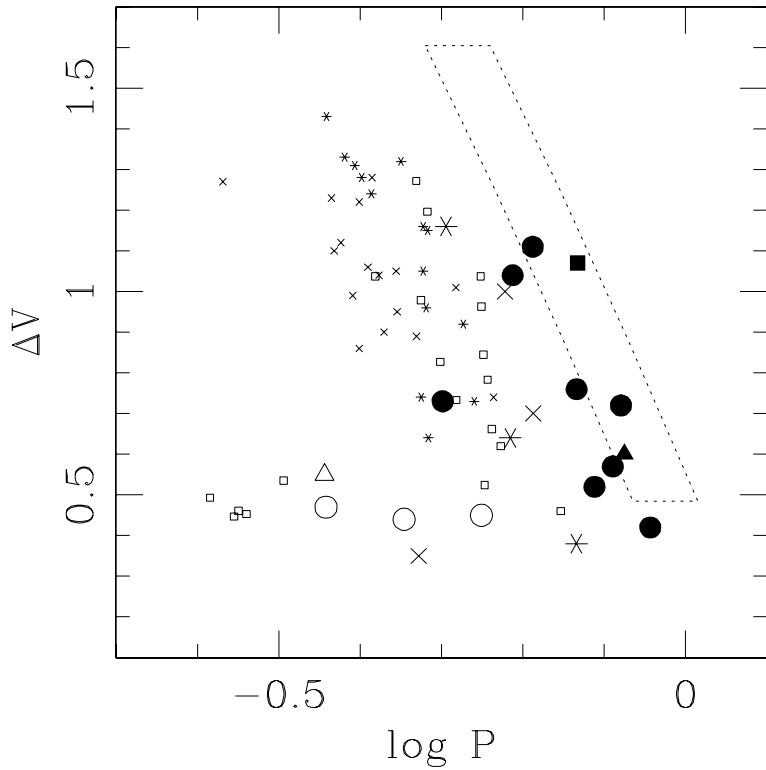


Fig. 9.— The Period-Amplitude diagram for metal-rich RR Lyrae stars. The small symbols include ab-type field RRL with  $[Fe/H] > -0.5$  ( $\times$ ), field RRL with  $-1.0 < [Fe/H] < -0.5$  (\*), and ab- and c-type RRL in NGC 6171 (Dickens 1970,  $\square$ ). Large symbols include: NGC 6441 variables V36, V41, and V44 (\*); SV2, SV3, and SV5 ( $\circ$ ); and the other RRL from Table 3 ( $\bullet$ ); 47 Tuc variable V9 (RRab, *solid square*); NGC 6388 variables V28 (RRab, *solid triangle*) and V27 (RRc, *open triangle*) from Silbermann et al. (1994). The dotted region represents one of the model predictions of Sweigart & Catelan (1998, from their Figure 3).

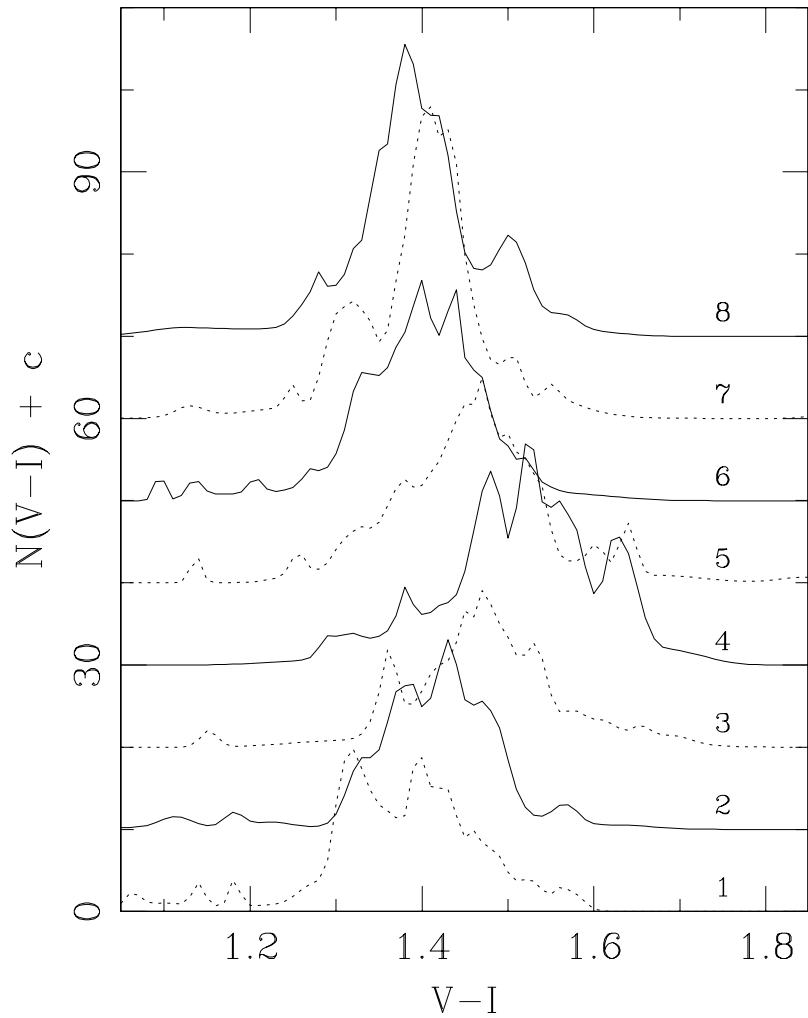


Fig. 10.— Generalized color histograms of red clump stars in the eight sectors numbered in the figure (see Table 7). Each histogram is a sum of unit-area Gaussian curves placed at the  $V - I$  color of each star and having a width equal to the color error of the star. The shifts between sectors indicate the presence and degree of differential reddening.

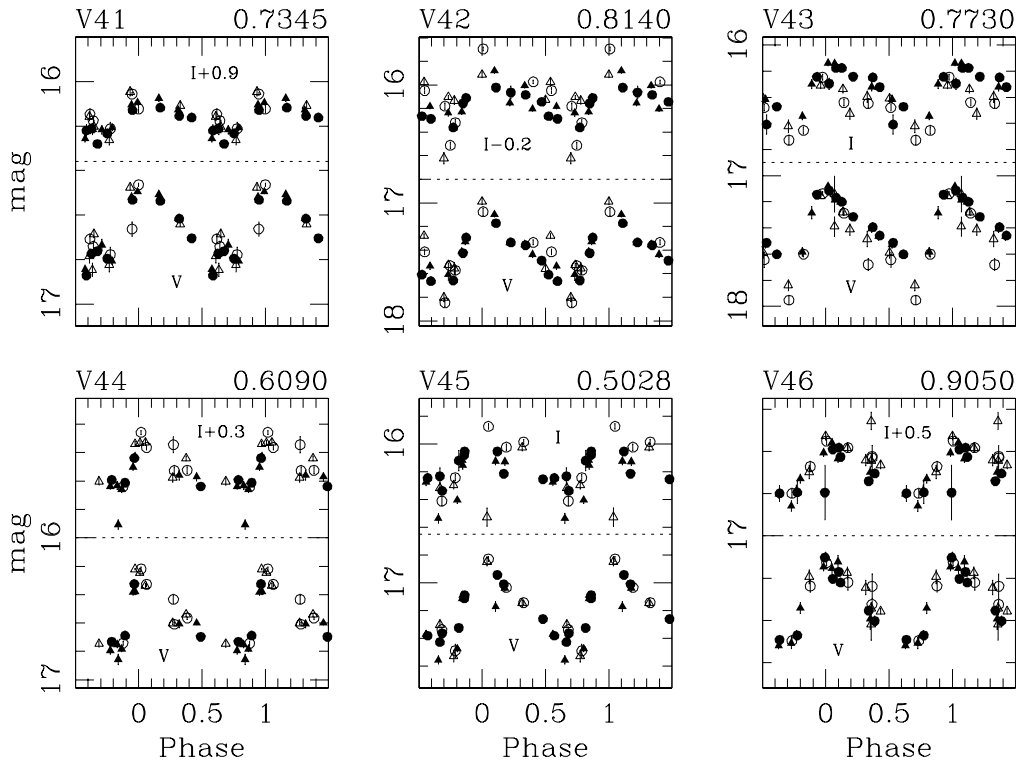


Fig. 12.— Additional light curves, continued from Figure 5.

This figure "layden\_fig1.jpg" is available in "jpg" format from:

<http://arxiv.org/ps/astro-ph/9808353v1>

This figure "layden\_fig2.jpg" is available in "jpg" format from:

<http://arxiv.org/ps/astro-ph/9808353v1>

This figure "layden\_fig3.jpg" is available in "jpg" format from:

<http://arxiv.org/ps/astro-ph/9808353v1>

This figure "layden\_fig4.jpg" is available in "jpg" format from:

<http://arxiv.org/ps/astro-ph/9808353v1>

This figure "layden\_fig7.jpg" is available in "jpg" format from:

<http://arxiv.org/ps/astro-ph/9808353v1>

This figure "layden\_fig11.jpg" is available in "jpg" format from:

<http://arxiv.org/ps/astro-ph/9808353v1>